Available online at www.sciencedirect.com

ScienceDirect

Ceramics International 40 (2014) 1531–1538

CERAMICS INTERNATIONAL

www.elsevier.com/locate/ceramint

# Hydrothermal synthesis and characterization of mesoporous rod-like hybrid organic-inorganic nanocrystalline based vanadium oxide

L. Soltane[a], F. Sediri[a,b,*]

[a]Laboratory of Condensed Matter Chemistry, IPEIT, University of Tunis 2, Jawaher Lel Nehru 1008, BP 229 Montfleury, Tunisia
[b]Chemistry Department, Sciences Faculty of Tunis, Tunis El Manar University, 2092El Manar, Tunisia

Received 4 July 2013; received in revised form 7 July 2013; accepted 8 July 2013
Available online 18 July 2013

**Abstract**

We describe a simple route to mesoporous rod-like nanocrystalline of hybrid organic–inorganic based vanadium oxide through the hydrothermal method using $V_2O_5$ as vanadium source and 2-phenylethylamine as reducing and structure-directing agent. Techniques X-ray diffraction (XRD), scanning electron microscope (SEM), thermal analysis (TG-DTA), X-ray photoelectron spectroscopy (XPS), Fourier transform infrared spectroscopy (FTIR), Raman spectroscopy, UV–visible spectroscopy and nitrogen adsorption/desorption isotherms (BET) have been used to characterize the structure, morphology and the texture of the samples. The nanorods are up to several hundred nanometers in length, the width and the thickness are 280–300 and 60 nm, respectively. The molar ratio plays a key role on the structure and the morphology of the materials.


*Keywords:* A. Hydrothermal synthesis; B. X-ray methods; D. Transition metal oxides

## 1. Introduction

Vanadium oxides have been extensively studied for their interesting physicochemical properties such as electrochemical performance [1–3]; a high capacity for lithium insertion makes it attractive to be used as cathodes in high-capacity batteries [4–8]; as well as in the field of catalysis [9,10]. The wide range of oxidation state and coordination polyhedra in the system vanadium/oxygen and the use of soft chemical process, in particular the mild hydrothermal method (120–250 °C) allows the synthesis of large amounts of vanadium oxide with open structure intercalated simple cation metal or organic molecules. Recently, several studies have been reported on the hydrothermal synthesis of hybrids organic-vanadium oxides materials using linear diamines molecules [11–16] ammonium cations [17–22] or alkyloviologen [23]. The organic molecules are sandwiched between the inorganic frameworks, where this latter has a lamellar structure formed by vanadium oxide layers with negative charge. The negative charges are then balanced by cations present in the interlayer space. More, pH plays a critical role in the formation of structure layers and the coordination of vanadium centers. Indeed, the vanadium may exhibit both $V^{4+}$ and $V^{5+}$ oxidation states and the layers are currently built from $[VO_5]$ square pyramids and $[VO_4]$ tetrahedral, at a pH close to 7 [24].

Furthermore, the physicochemical properties of solid state materials mainly depend on their size, structure and morphology [25]. Subsequently, nanostructured materials have attracted considerable attention due to their remarkable physicochemical properties, which differs considerably to dense materials, thereafter their use in great potential applications [26–28]. Among them, one-dimensional (1D) nanostructure vanadium oxides, such as nanotubes, nanowires, nanobelts and nanorods, have been extensively studied the past few years [25,29–33].

*Corresponding author at: Tunis El Manar University, Chemistry Department, Sciences Faculty of Tunis, El Manar 2092, Tunisia. Tel.: +216 71336641; fax: +216 71337323.
*E-mail addresses:* faouzi.sediri@ipeit.rnu.tn, sediri68@gmail.com (F. Sediri).

0272-8842/$ - see front matter © 2013 Elsevier Ltd and Techna Group S.r.l. All rights reserved.
http://dx.doi.org/10.1016/j.ceramint.2013.07.039

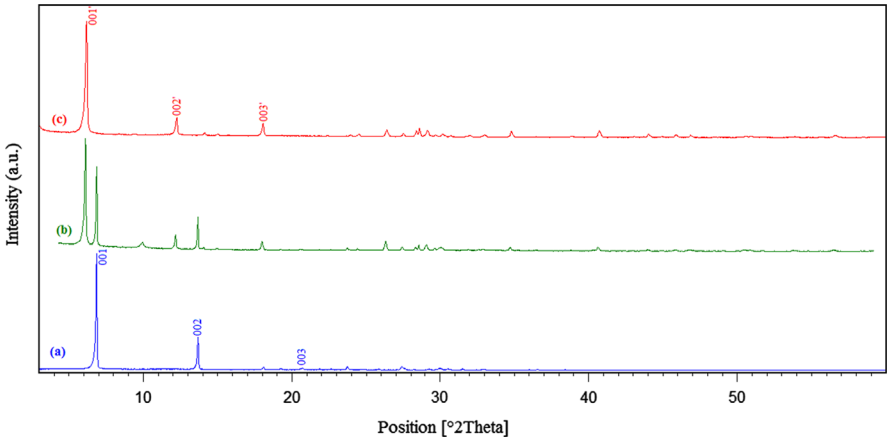


Fig. 1. Powder X-ray diffraction patterns of the resulting products synthesized at different molar ratio $V_2O_5$:2-phenylethylamine (a) 1:1, (b) 0.5:1 and (c) 2:1.

This paper deals with the synthesis of rod-like hybrid organic–inorganic nanocrystalline based vanadium oxide by hydrothermal reaction of $V_2O_5$ as a vanadium source and 2-phenylethylamine which acts as structure-directing, size and morphology-controlling agent. The impact of the molar ratio on the particles size and the morphology has been investigated. Although many methods have been developed to elaborate hybrid organic-inorganic nanocrystalline based vanadium oxide, to the best of our knowledge, this is the first report of hybrid organic–inorganic nanomaterial based vanadium oxide synthesis using $V_2O_5$ and 2-phenylethylamine as a structure-directing template.

## 2. Experimental section

### 2.1. Characterization techniques

X-ray powder diffraction data (XRD) were obtained on a X'Pert Pro Panalytical diffractometer with CuKα radiation ($\lambda$=1.5418 Å) and graphite monochromator. The XRD measurements were carried out by applying a step scanning method ($2\theta$ range from 3° to 59.98°), the scanning rate is 0.017 $s^{-1}$ and the step time is 12 s. Scanning electron microscopy (SEM) studies were recorded on a Cambridge Instruments Stereoscan 120 at an accelerating voltage of 10 kV. Fourier-transform infrared spectra (FTIR) were recorded from 4000 to 400 $cm^{-1}$ on a Nicolet 380 spectrometer in pellets of samples dispersed in KBr. Raman spectroscopy was performed using a Jobin Yvon T 64000 spectrometer (blue laser excitation with 488 nm wavelength and $<55$ mW power at the sample). Thermogravimetric analyses were carried out under an oxygen flux of 5 $cm^3$ $min^{-1}$ at a heating rate of 10 °C $min^{-1}$ between room temperature and 600 °C, using a Netsch STA 409 thermogravimetric analyzer. X-ray photoelectron spectroscopy (XPS) experiments were performed using a Shimadzu ESCALAB, at room temperature. The optical parameters of sample were calculated from the optical absorbance data recorded in the wavelength range from 200 to 800 nm using a UV–visible spectrophotometer Shimadzu-3101PC.

### 2.2. Hydrothermal synthesis

All of the chemical reagents were analytical grade. They were purchased from Acros Organics and used without further purification.

The detailed process for the synthesis was as follows. In a typical synthesis, the preparation was made from a mixture of $V_2O_5$, 2-phenylethylamine and distilled water (5 mL) at different molar ratio of $V_2O_5$ to 2-phenylethylamine. Reactants were introduced in this order and stirred a few hours before introducing the resulting mixture in a Teflon-lined steel autoclave and the temperature set at 180 °C for 2 days under autogenous pressure. The pH of the reaction mixture remains close to pH≈10. The resulting black powder was washed with water and acetone to remove the residues of 2-phenylethylamine and then dried at 80 °C for 6 h. The black color of the powder suggests that some $V^{5+}$ ions have been reduced to $V^{4+}$ by the decomposition of the organic compound [34]. Comparative experiments were carried out to investigate the influence of the molar ratio of $V_2O_5$ to 2-phenylethylamine on the crystallinity, morphology and texture of the materials.

## 3. Results and discussion

### 3.1. X-ray diffraction

The crystallinity of the resulting samples synthesized at 180 °C for different molar ratio of $V_2O_5$ to 2-phenylethylamine (a) 0.5:1, (b) 1:1 and (c) 2:1, were studied by X-ray powder diffraction (XRD), as shown in Fig. 1. It is obvious that the crystalline phases for vanadium oxide nanocrystals are discriminatory at different molar ratios. Indeed, when the molar ratio $R$=0.5:1 (Fig. 1a), the patterns predominantly consist of a series of peaks with high intensity corresponding to the stacking of the layers along a direction perpendicular to the substrate which have d-spacings of the type $d_{001}$/l, where l is

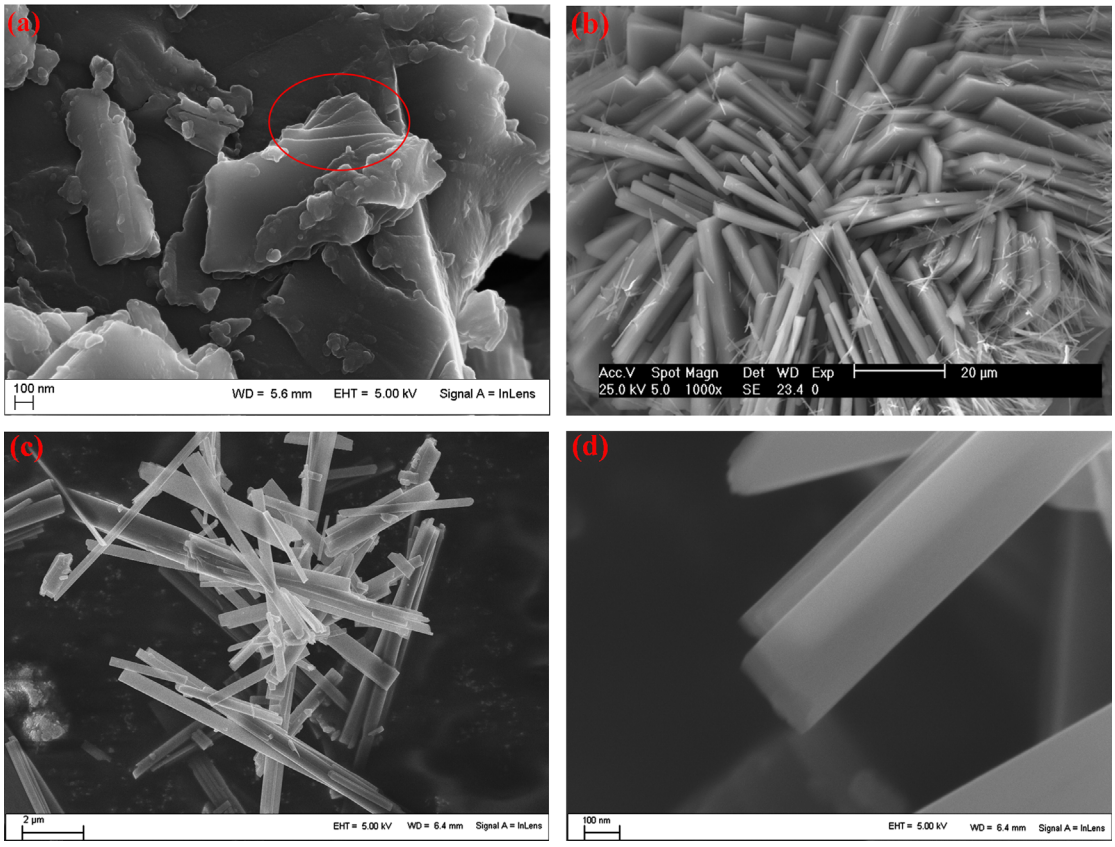


Fig. 2. SEM micrographs of the resulting products synthesized at different molar ratio $V_2O_5$:2-phenylethylamine (a) 0.5:1, (b) 1:1 and (c and d) 2:1.

an integer, and that is a strong indication of the occurrence of lamellar structure [16,35]. The 00l series provided the distance between the vanadium oxide layers (e.g. $d_{00l}$=1.287 nm). However, when the molar ratio $R$=1:1, it was possible to distinguish an additional 00l′ series of reflections whose basal distance was close to 1.445 nm. This second series may be assigned to another lamellar stacking. In fact, the X-ray diffraction pattern displayed the formation of a lamellar compound with a stacking defect. This behavior can be attributed to two different orientations of organic molecules between the vanadium oxide layers, where their presence has been confirmed by infrared spectroscopy. Besides, when the molar ratio $R$=2:1, the XRD patterns shown in Fig. 1c indicates that the d-spacing values of all diffraction peaks are characteristic of well-ordered lamellar compound. The 00l′ series provided the distance between the vanadium oxide layers (e.g. $d_{00l}$=1.445 nm).

Vanadium oxides with mixed valency, containing $V^{5+}$ as well as $V^{4+}$ cations, were usually obtained by hydrothermal processing of precursor and reductive organic molecules [36]. In the present study, during the hydrothermal synthetic process from the $V_2O_5$, the 2-phenylethylamine served as a template as well as a reducing agent. The products were in black color after the hydrothermal process, which indicates $V^{5+}$ cations partially reduced to $V^{4+}$ cations. The 2-phenylethylamine played a critical role in the formation of the lamellar hybrid materials based vanadium oxide during the hydrothermal process.

The average crystallite size of the as-synthesized materials was calculated by using Scherrer's formula:

$$L = \frac{0.89\lambda}{\beta \cos\ \theta}$$

where $L$ is the average crystallite size, $\lambda$=0.15418 nm, $\beta$ is the half maximum peak width and $\theta$ is the diffraction angle in degrees [37]. The average crystallite size values, calculated from XRD patterns of the samples synthesized with the molar ratio 0.5:1, 1:1 and 2:1, have been found to be, about 119, 111 and 95 nm, respectively.

### 3.2. Scanning electron microscopy

The morphology evolution of the samples was carried out with respect to different molar ratio of $V_2O_5$ to 2-phenylethylamine. Indeed, the morphology of synthesized samples was studied by using the scanning electron microscopy (SEM). It was found that the molar ratio plays a critical role in the morphology and leads to the different morphologies of samples as shown in SEM micrographs (Fig. 2). Indeed, when the molar ratio $R$=0.5:1, the SEM image of the material reveals the layered morphology with stratified structure (Fig. 2a). However, when the molar ratio $R$=1:1 was used, the synthesized sample had a nearly only square platelets as thick as 1 µm, as shown in Fig. 2b. With increasing the molar ratio to 2:1, the micrographs show a change in the morphology

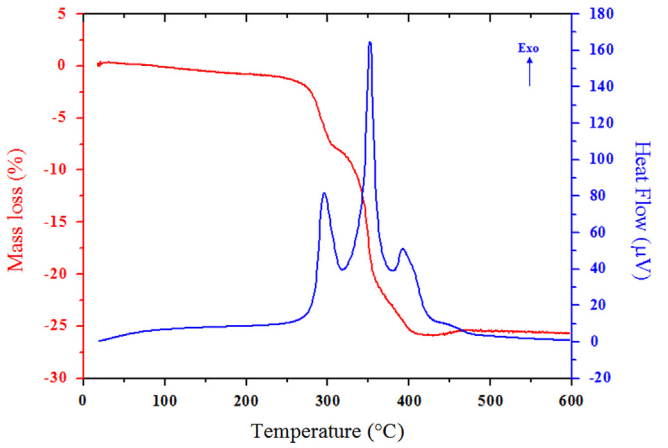


Fig. 3. Thermal analysis of the hybrid organic–inorganic nanorods.

of the sample. Indeed, the SEM images shown in Fig. 2c–d indicates that with a $V_2O_5$:2-phenylethylamine ratio of 2:1 the material consists of a homogenous phase of uniform nanorods. Dimensions of these nanorods found from SEM images are about 60 nm in thickness, 280–300 nm in width, and several micrometers in length. As reported in the literature, organic molecules were found to play an important role in the controlling the morphologies [38,39]. In view of these results, we can conclude that 2-phenylethylamine plays important role on the types of structure and the morphology of the product.

### 3.3. Thermal analysis

The thermal stability of the as-synthesized hybrid organic–inorganic nanorods was studied by carrying out TG and DTA analysis (Fig. 3). Thermogravimetric analyses show that the sample contains almost no water. A large weight loss is observed between 260 and 400 °C corresponding to the combustion of organic molecules (26% in weight). It is associated with three exothermic peaks in DTA. The remaining 74% in weight corresponds to vanadium oxide. A slight increase in weight corresponding to an exothermic DTA peak occurs around 400 °C. It could be assigned to the oxidation of $V^{4+}$ into $V^{5+}$ leading to the formation of the yellow crystalline $V_2O_5$ [JCPDS 89-2482].

### 3.4. Infrared spectroscopy

The Fourier Transform Infrared (FT-IR) spectra of post hydrothermal treated samples of $V_2O_5$:2-phenylethylamine = 1:1 and 2:1 are shown in Fig. 3. For $V_2O_5$:2-phenylethylamine = 1:1, the infrared spectrum of the material (Fig. 4a) exhibits the bands at 2966, 2931, 2851 and 1511 $cm^{-1}$, which could be assigned to the stretching and bending modes of the different C–H vibrations in the 2-phenylethylamine [40]. The band around 3195 $cm^{-1}$ corresponds to the stretching vibrations of N–H bonds in the $NH_3^+$ group [41]. The broad band at 3436 $cm^{-1}$ corresponds to the OH groups coordinated to the vanadium, whereas the bending vibrations of water molecules become visible as a narrow band at 1609 $cm^{-1}$, which might indicate that a certain amount of water molecules

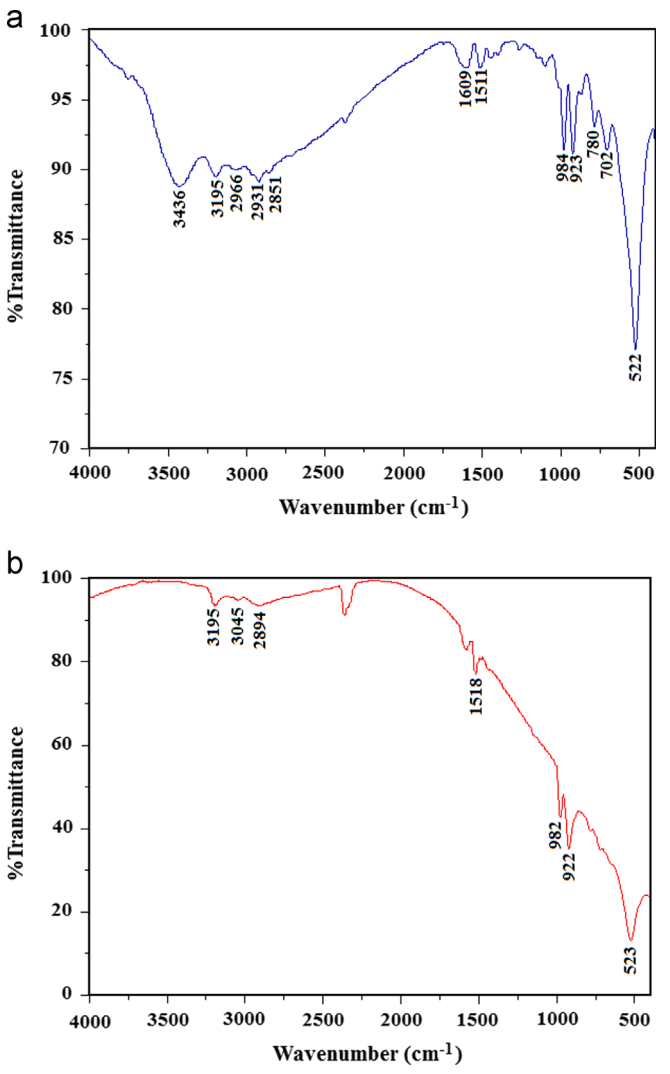


Fig. 4. IR spectra of the resulting materials synthesized at different molar ratio $V_2O_5$:2-phenylethylamine (a) 1:1 and (b) 2:1.

is embedded between the layers [42]. The bands vibrations of different V–O vibrator are observed below 1100 $cm^{-1}$. Indeed, the bands at 984 $cm^{-1}$ and 923 $cm^{-1}$ correspond to the symmetric stretching vibration of the νs ($V^{5+}=O$) and νs ($V^{4+}=O$) bonds, respectively [42]. The bands at 522, 702 and 780 $cm^{-1}$ can be assigned to the V–O–V symmetric and asymmetric stretching vibration, respectively [43]. The FTIR results show intercalation reaction of 2-phenylethylamine and $V_2O_5$ [44]. However, for $V_2O_5$:2-phenylethylamine = 2:1, the infrared spectrum of the nanorods (Fig. 3b) reveals the disappearance of the related water molecules bonds which has been confirmed by thermogravimetric analysis. Furthermore, the infrared spectrum confirms that the product contains organic molecules. Indeed, the Fig. 4b reveals adsorptions bands at 3195, 3045, 2894 and 1518 $cm^{-1}$, which could be assigned to the stretching and bending modes of the different $[-NH_3]^+$ and C–H vibrations in 2-phenylethylamine cation, respectively. All the vibration modes occurring below 1100 $cm^{-1}$ can be attributed to the inorganic network. Indeed, the bands at 982 and 923 $cm^{-1}$ are attributed to the symmetric

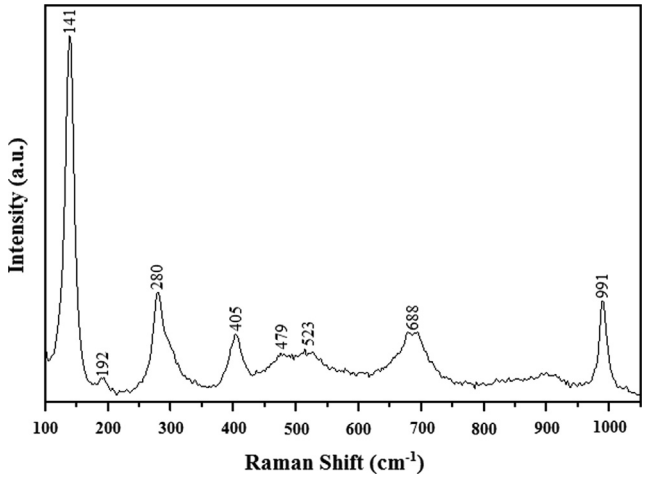


Fig. 5. Raman spectrum of the hybrid organic–inorganic nanorods.

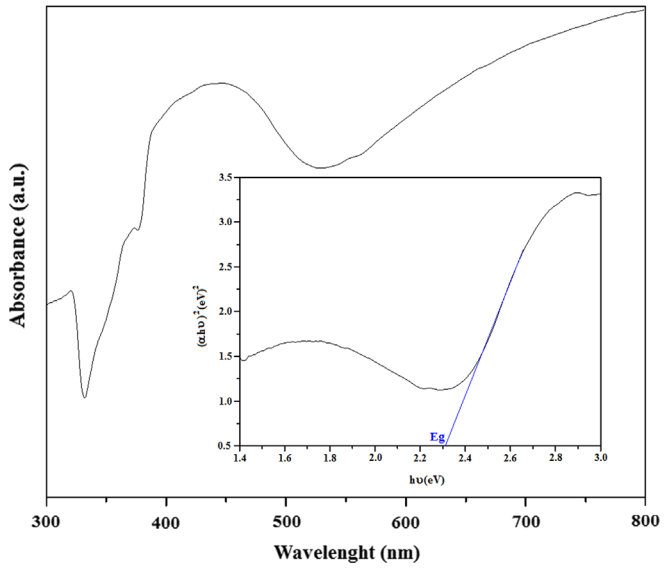


Fig. 6. UV–Visible absorption spectrum and the $(\alpha h\nu)^2$ versus $h\nu$ plot (inset) of the hybrid organic–inorganic nanorods.

stretching of the νs ($V^{5+}$=O) and νs ($V^{4+}$=O) bonds, respectively. The broad band located at 523 $cm^{-1}$ is assigned to V–O–V stretching modes [45].

### 3.5. Raman spectroscopy

A typical room temperature Raman spectrum of the nanorods is shown in Fig. 5. In fact, the spectrum displays a series of Raman band in the range of 100–1000 $cm^{-1}$, which is due to the various (group) vibrations of V–O type. The low wavenumber modes can be described in terms of external modes. Indeed, two low-frequency Raman bands located at 192 $cm^{-1}$ ($B_{1g}$ mode) and 141 $cm^{-1}$ ($B_{3g}$, $B_{2g}$ symmetry) which are assigned to the stretching mode of $(V_2O_2)_n$ correspond to the chain translation [46,47]. These bands are strongly associated with the layered structure which is in agreement with the XRD results. Moreover, the sharp, strong and dominant band observed at 141 $cm^{-1}$ indicates that the crystalline product has a very long-range order [47,48]. On the other hand, the internal modes are observed in the medium and high wavenumber region can be described in terms of O–V–O and V–O–V bending modes and V–O stretching modes [46]. Indeed, the bands observed at 280 ($B_{2g}$, $B_{3g}$) and 405 $cm^{-1}$ ($A_g$) are assigned to the bending vibration of the $O_3$–V=O bonds and to the bending vibration of the V–$O_3$–V, respectively [47,49]. The band situated at 480 $cm^{-1}$ ($A_g$) is attributed to the bending vibration of the bridging V–$O_2$–V [47]. However, the band at 524 $cm^{-1}$ ($A_g$) is assigned to the triply coordinated oxygen ($V_3$–O) stretching mode [46,49]. Nevertheless, the band located at 688 $cm^{-1}$ ($B_{2g}$, $B_{3g}$) is assigned to the stretching vibration of the doubly coordinated oxygen ($V_2$–O) [46–50]. While, the high frequency Raman band situated at 991 $cm^{-1}$ ($A_g$ symmetry) corresponds to the terminal oxygen (V=O) stretching mode which results from an unshared oxygen [47,49]. Therefore, the Raman active modes can be described as follows: $4A_g+B_{1g}+3B_{2g}+3B_{3g}$.

### 3.6. UV–vis spectroscopy

The optical properties of as-obtained hybrid organic–inorganic nanorods were investigated by UV–visible spectroscopy. The absorption spectrum of the nanorods is shown in Fig. 6. It is well-known that the maxima band of O→$V^{n+}$ charge transfer transition depends on the number of O atoms surrounding the central vanadium ion [51,52]. Therefore, $V^{5+}$ in tetrahedral coordination absorbs in the range 240–350 nm, in square pyramidal coordination at 350–450 nm and in octahedral coordination at 450–600 nm [51,52]. In fact, the UV–vis spectrum shows a weak absorption band at around 318 nm which can be attributed to lower energy charge transfer to $V^{5+}$ species in tetrahedral coordination [51]. Another weak band located at 360 nm can be attributed to the $n\rightarrow\pi^*$ transition centered on the V=O group in square pyramidal coordination [51]. However, the spectrum a exhibits a large absorption band centered at around 430 nm was shifted to shorter wavelengths (blue-shift) compared to that of bulk $V_2O_5$ powders (470–500 nm) [16,53]. This band can be attributed to the electron transfer from oxygen atoms to vanadium in octahedral coordination [54]. The origin of this change of spectral band position was suggested to be the contribution of a quantum size effect in the hybrid nanorods [50,55].

The optical band gap, $E_g$, can be estimated from the following equation known as the Tauc plot [56]:

$$\alpha h\nu = (h\nu - E_g)^n$$

where $n$ is an exponent, $\nu$ is the frequency of the incident radiation, $h$ is the Plank's constant, and $E_g$ is the optical energy gap of the material. The exponent $n$ can take the values 2, 3, 1/2 and 3/2 for indirect allowed, indirect forbidden, direct allowed and direct forbidden transitions, respectively [56,57]. Plotting of $(\alpha h\nu)^{1/n}$ versus $(h\nu)$ and extrapolating to $(\alpha h\nu)^{1/n}$=0 yields the value of $E_g$. In the inset in Fig. 6, as example the plot of $(\alpha h\nu)^2$ versus photon energy $(h\nu)$ for the nanorods is shown; the results obey the above equation with $n$=1/2 indicating direct allowed

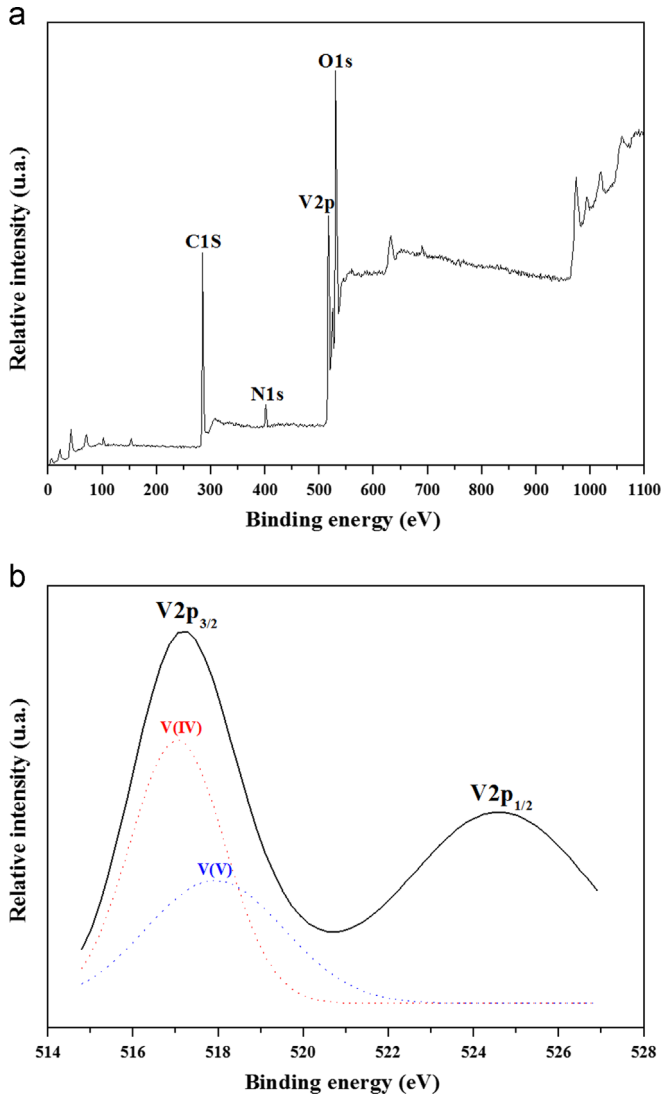


Fig. 7. XPS of the hybrid organic-inorganic nanorods: (a) survey spectrum and (b) core level spectrum of V2p.

transition and correspond to $E_g = 2.31$ eV. The optical band gap of 2.31 eV can be attributed to direct transition from occupied 2p bands of oxygen to unoccupied 3d bands of vanadium [56,57].

### 3.7. X-ray photoelectron spectroscopy

The composition and vanadium valence state of the surface of the as-synthesized nanorods were further investigated by X-ray photoelectron spectroscopy (XPS), as shown in Fig. 7a the typical XPS survey spectrum of the as-synthesized nanorods and the fitted-curves about $V2p_{3/2}$ and $V2p_{1/2}$ are illustrated in Fig. 7b. The XPS survey spectrum reveals that the sample only consists of carbon, nitrogen, vanadium and oxygen. The core level binding energies of $V2p_{3/2}$ and $V2p_{1/2}$ spectra are located at 517.93 and 524.59 eV, respectively. The $V2p_{3/2}$ peak of the sample is divided into two peaks at the binding energies of 516.88 and 517.75 eV, assigned to $V^{4+}$ and $V^{5+}$, respectively [58,59]. Therefore, the core-level spectra

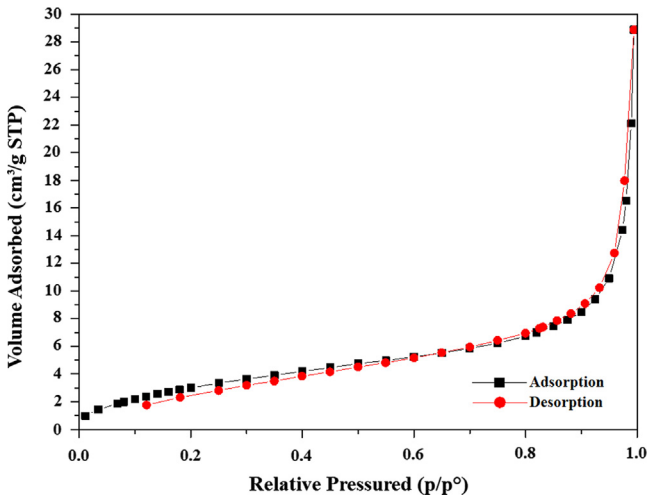


Fig. 8. N2 absorption/desorption isotherms of the hybrid organic-–inorganic nanorods.

of V2p further confirm that the as-synthesized nanorods consist of $V^{5+}$ and $V^{4+}$.

### 3.8. Nitrogen adsorption

The specific BET surface area ($S_{BET}$), pore volume ($V_{por}$) and average pore size ($d_{por}$) of the hybrid organic-inorganic nanorods were measured by physisorption of nitrogen according to the Brunauer–Emmett–Teller (BET) method. The following results are noticed: $S_{BET}$=11 $m^2\,g^{-1}$, $V_{por}$=22.$10^{-3}$ $cm^3\,g^{-1}$ and $d_{por}$=71 Å. It is known to all that many chemical and physical properties of products deeply depend on both initial material size and the synthetic method. Moreover, $N_2$ adsorption–desorption isotherms of the sample (Fig. 8) exhibits IV-type hysteresis loops which are characteristics of mesoporous materials having pore diameter between 2 and 50 nm [60,61]. This result is confirmed by the specific surface area and the average pore size values. IV-type hysteresis loops are usually observed with rigid bulk particles having a uniform sizes.

## 4. Conclusion

In summary, mesoporous rod-like nanocrystalline of well-ordered layered structure hybrid organic–inorganic based vanadium oxide intercalated by 2-phenylethylamine was synthesized through mild hydrothermal process. The layered structure with an inter layer distance of 1.445 nm was confirmed by X-ray diffraction patterns. In fact, the presence of organic molecules and the vanadium valence state were confirmed by FTIR spectroscopy, thermal analysis and XPS measurements. The rod-like nanostructure in this study has high crystallinity with the mean width of 280–300 nm, thickness of 60 nm and surface area 11 $m^2\,g^{-1}$. The optical properties of the as-synthesized nanorods were investigated by UV–visible spectroscopy. As a result, the optical band gap was found to be 2.31 eV and attributed to direct transition from

occupied 2p bands of oxygen to unoccupied 3d bands of vanadium.

## References


[1] C. Cui, G. Wu, H. Yang, S. She, J. Shen, B. Zhou, Z. Zhang, A new high-performance cathode material for rechargeable lithium-ion batteries: polypyrrole/vanadium oxide nanotubes, Electrochimica Acta 55 (2010) 8870–8875.

[2] Y. Wang, G. Cao, Synthesis and enhanced intercalation properties of nanostructured vanadium oxides, Chemistry of Materials 18 (2006) 2787–2804.

[3] Y. Wang, G. Cao, Developments in nanostructured cathode materials for high-performance lithium-ion batteries, Advanced Materials 20 (2008) 2251–2269.

[4] C. Ban, N.A. Chernova, M.S. Whittingham, Electrospun nano-vanadium pentoxide cathode, Electrochemistry Communications 11 (2009) 522–525.

[5] J. Xu, H. Zhang, T. Zhang, Q. Pan, Y. Gui, Influence of heat-treatment temperature on crystal structure, morphology and electrochemical properties of $LiV_3O_8$ prepared by hydrothermal reaction, Journal of Alloys and Compounds 467 (2009) 327–331.

[6] C. Cui, G. Wu, J. Shen, B. Zhou, Z. Zhang, H. Yang, S. She, Synthesis and electrochemical performance of lithium vanadium oxide nanotubes as cathodes for rechargeable lithium-ion batteries, Electrochimica Acta 55 (2010) 2536–2541.

[7] Y. Wang, K. Takahashi, K. Lee, G. Cao, Nanostructured vanadium oxide electrodes for enhanced lithium-ion intercalation, Advanced Functional Materials 16 (2006) 1133–1144.

[8] T.M. Benedetti, E. Redston, W.G. Menezes, D.M. Reis, J.F. Soares, A.J. G. Zarbin, R.M. Torresi, Lithium intercalation in nanostructured thin films of a mixed-valence layered vanadium oxide using an ionic liquid electrolyte, Journal of Power Sources 224 (2013) 72–79.

[9] A. Held, P. Florczak, Vanadium, niobium and tantalum modified mesoporous molecular sieves as catalysts for propene epoxidation, Catalysis Today 142 (2009) 329–334.

[10] J.K. Joseph, S. Singhal, S.L. Jain, R. Sivakumaran, B. Kumar, B. Sain, Studies on vanadium catalyzed direct hydroxylation of aromatic hydrocarbons using hydrogen peroxide as oxidant, Catalysis Today 141 (2009) 211–214.

[11] Y. Zhang, C.J. O'Connor, A. Clearfield, R.C. Haushalter, An organically templated layered vanadium oxide: hydrothermal synthesis, single-crystal structure, and magnetic properties of $(H_3N(CH_2)_3NH_3)[V_4O_{10}]$, Chemistry of Materials 8 (1996) 595–597.

[12] D. Riou, G. Férey, Intercalated vanadyl vanadate (VIVO)[VVO4].0.5 [C3N2H12]: hydrothermal synthesis, crystal structure, and structural correlations with $V_2O_5$ and other vanadyl compounds, Journal of Solid State Chemistry 120 (1995) 137–145.

[13] F. Sediri, N. Etteyeb, N. Gharbi, N. Steunou, J. Livage, Hydrothermal synthesis of $(H_3N(CH_2)_3NH_3)[V_4O_{10}]$, Annales de Chimie—Science des Matériaux 28 (2003) 129–134.

[14] D. Riou, G. Férey, Hydrothermal synthesis and structure determination of 1,4-diaminobutane metavanadate, Journal of Solid State Chemistry 124 (1996) 151–154.

[15] D. Riou, G. Férey, Intercalated vanadyl vanadates: syntheses, crystal structures, and magnetic properties, Inorganic Chemistry 34 (1995) 6520–6523.

[16] S. Cheng, H. Hwang, G.E. Maciel, Synthesis and pillaring of a layered vanadium oxide from $V_2O_5$ at ambient temperature, Journal of Molecular Structure 470 (1998) 135–149.

[17] S.T. Lutta, N.A. Chernova, P.Y. Zavalij, M.S. Whittingham, Synthesis, crystal structures and magnetic properties of organically templated new layered vanadates: $[C_4H_8NH_2]V_3O_7$, $[(CH_3)_2NH_2]V_3O_7$, $[C_5H_{10}NH_2]V_3O_7$ and $[C_2H_5NH_3]V_3O_7$, Journal of Materials Chemistry 14 (2004) 2922–2928.

[18] M.S. Whittingham, J. Guo, R. Chen, T. Chirayil, G. Janauer, P. Zavalij, Hydrothermal synthesis of new oxide materials, Solid State Ionics 75 (1995) 257–268.

[19] E.A. Boylan, T. Chirayil, J. Hinz, P.Y. Zavalij, M.S. Whittingham, Vanadium oxides synthesized using the tetramethylammonium ion: an addendum, Solid State Ionics 90 (1996) l–4.

[20] Chunmei Ban, M. Stanley Whittingham, Nanoscale single-crystal vanadium oxides with layered structure by electrospinning and hydrothermal methods, Solid State Ionics 179 (2008) 1721–1724.

[21] F.J. Quites, C. Bisio, R.G. Vinhas, R. Landers, L. Marchese, H.O. Pastore, Vanadium oxide intercalated with polyelectrolytes. novel layered hybrids with anion exchange properties, Journal of Colloid and Interface Science 368 (2012) 462–469.

[22] S.G. Leonardi, P. Primerano, N. Donato, G. Neri, Behavior of sheet-like crystalline ammonium trivanadate hemihydrate (NH4V3O8 × 0.5H2O) as a novel ammonia sensing material, Journal of Solid State Chemistry 202 (2013) 105–110.

[23] K. Lai, A. Kong, F. Yang, B. Chen, H. Ding, Y. Shan, S. Huang, Intercalation of alkylviologen dications into the layered vanadium pentoxide, Inorganica Chimica Acta 359 (2006) 1050–1054.

[24] F. Sediri, N. Etteyeb, N. Steunou, C. Guyard-Duhayon, J. Maquet, N. Gharbi, J. Livage, Hydrothermal synthesis and characterization of $(H_3N(CH_2)_4NH_3)[V_6O_{14}]$, Journal of Solid State Chemistry 167 (2002) 407–411.

[25] J. Livage, Hydrothermal synthesis of nanostructured vanadium oxides, Matter 3 (2010) 4175–4195.

[26] A. Pan, H.B. Wu, L. Yu, T. Zhu, X.W. Lou, Synthesis of hierarchical three-dimensional vanadium oxide microstructures as high-capacity cathode materials for lithium-ion batteries, ACS Applied Materials and Interfaces 4 (2012) 3874–3879.

[27] D. Wei, M.R.J. Scherer, C. Bower, P. Andrew, T. Ryhänen, U. Steiner, A nanostructured electrochromic supercapacitor, Nano Letters 12 (2012) 1857–1862.

[28] H.A. Abbood, H. Peng, X. Gao, B. Tan, K. Huang, Fabrication of cross-like $NH_4V_4O_{10}$ nanobelt array controlled by CMC as soft template and photocatalytic activity of its calcinated product, Chemical Engineering Journal 209 (2012) 245–254.

[29] N. Pinna, U. Wild, J. Urban, R. Schlögl, Divanadium pentoxide nanorods, Advanced Materials 15 (2003) 329–331.

[30] N. Pinna, W. Willinger, K. Weiss, J. Urban, R. Schlögl, Local structure of nanoscopic materials: $V_2O_5$ nanorods and nanowires, Nano Letters 3 (2003) 1131–1134.

[31] S. Pavasupree, Y. Suzuki, A. Kitiyanan, S. Pivsa-Art, S. Yoshikawa, Synthesis and characterization of vanadium oxides nanorods, Journal of Solid State Chemistry 178 (2005) 2152–2158.

[32] L. Mai, L. Xu, C. Han, X. Xu, Y. Luo, S. Zhao, Y. Zhao, Electrospun ultralong hierarchical vanadium oxide nanowires with high performance for lithium ion batteries, Nano Letters 10 (2010) 4750–4755.

[33] Y. Li, X.Y. Yang, Y. Feng, Z.Y. Yuan, B.L. Su, One-dimensional metal oxide nanotubes, nanowires, nanoribbons, and nanorods: synthesis, characterizations, properties and applications, Critical Reviews in Solid State and Materials Sciences 37 (2012) 1–74.

[34] L. Bouhedja, N. Stenou, J. Maquet, J. Livage, Synthesis of polyoxovanadates from aqueous solutions, Journal of Solid State Chemistry 162 (2001) 315–321.

[35] M. Jaber, F. Ribot, L. Binet, V. Briois, S. Cassaignon, K.J. Rao, J. Livage, N. Steunou, Ex Situ X-ray diffraction, X-ray absorption near edge structure, electron spin resonance, and transmission electron microscopy study of the hydrothermal crystallization of vanadium oxide nanotubes: an insight into the mechanism of formation, Journal of Physical Chemistry C 116 (2012) 25126–25136.

[36] I. Mjejri, N. Etteyeb, F. Sediri, Hydrothermal synthesis of mesoporous rod-like nanocrystalline vanadium oxide hydrate $V_3O_7 \cdot H_2O$ from hydroquinone and $V_2O_5$, Materials Research Bulletin 48 (2013) 3335–3341.

[37] R. Huang, Y. Shen, L. Zhao, M. Yan, Effect of hydrothermal temperature on structure and photochromic properties of $WO_3$ powder, Advanced Powder Technology 23 (2012) 211–214.

[38] F. Huang, H. Zhang, J.F. Banfield, Two-stage crystal-growth kinetics observed during hydrothermal coarsening of nanocrystalline ZnS, Nano Letters 3 (2003) 373–378.

[39] F. Sediri, N. Gharbi, From crystalline $V_2O_5$ to nanostructured vanadium oxides using aromatic amines as templates, Journal of Physics and Chemistry of Solids 68 (2007) 1821–1829.
[40] F. Sediri, F. Touati, N. Gharbi, A one-step hydrothermal way for the synthesis of vanadium oxide nanotubes containing the phenylpropylamine as template obtained via non-alkoxide route, Materials Letters 61 (2007) 1946–1950.
[41] A. Dobley, K. Ngala, S. Yang, P.Y. Zavalij, M.S. Whittingham, Manganese vanadium oxide nanotubes: synthesis, characterization, and electrochemistry, Chemistry of Materials 13 (2001) 4382–4386.
[42] W. Chen, J. Peng, L. Mai, Q. Zhu, Q. Xu, Synthesis of vanadium oxide nanotubes from $V_2O_5$ sols, Materials Letters 58 (2004) 2275–2278.
[43] B. Azambre, M.J. Hudson, O. Heintz, Topotactic redox reactions of copper(II) and iron(III) salts within $VO_x$ nanotubes, Journal of Materials Chemistry 13 (2003) 385–393.
[44] N. Asim, S. Radiman, M. bin Yarmo, Preparation and characterization of core-shell polyaniline/V2O5 nanocomposite via microemulsion method, Materials Letters 62 (2008) 1044–1047.
[45] F. Sediri, N. Gharbi, Nanorod B phase $VO_2$ obtained by using benzylamine as a reducing agent, Materials Science and Engineering: B 139 (2007) 114–117.
[46] G. Faggio, V. Modafferi, G. Panzera, D. Alfieri, S. Santangelo, Micro-Raman and photoluminescence analysis of composite vanadium oxide/poly-vinyl acetate fibres synthesised by electro-spinning, Journal of Raman Spectroscopy 43 (2012) 761–768.
[47] R. Baddour-Hadjean, V. Golabkan, J.P. Pereira-Ramos, A. Mantoux, D. Lincot, A Raman study of the lithium insertion process in vanadium pentoxide thin films deposited by atomic layer deposition, Journal of Raman Spectroscopy 33 (2002) 631–638.
[48] S.e.-H. Lee, H.M. Cheong, M.J. Seong, P. Liu, C.E. Tracy, A. Mascarenhas, J.R. Pitts, S.K. Deb, Raman spectroscopic studies of amorphous vanadium oxide thin films, Solid State Ionics 165 (2003) 111–116.
[49] R. Baddour-Hadjean, A. Marzouk, J.P. Pereira-Ramos, Structural modifications of $LixV_2O_5$ in a composite cathode ($0 \leq x < 2$) investigated by Raman microspectrometry, Journal of Raman Spectroscopy 43 (2012) 153–160.
[50] N. Rama, M.S.R. Rao, Synthesis and study of electrical and magnetic properties of vanadium oxide micro and nanosized rods grown using pulsed laser deposition technique, Solid State Communications 150 (2010) 1041–1044.
[51] J. Liu, D. Xie, Cation-induced coiling of vanadium pentoxide nanobelts, Nanoscale Research Letters 5 (2010) 1619–1626.
[52] M.K. Chine, F. Sediri, N. Gharbi, Solvothermal synthesis of $V_4O_9$ flake-like morphology and its photocatalytic application in the degradation of methylene blue, Materials Research Bulletin 47 (2012) 3422–3426.
[53] G. Nagaraju, P. Chithaiahb, S. Ashokac, N. Mahadevaiah, Vanadium pentoxide nanobelts: one pot synthesis and its lithium storage behavior, Crystal Research and Technology 47 (2012) 868–875.
[54] G. Li, S. Pang, L. Jiang, Z. Guo, Z. Zhang, Environmentally friendly chemical route to vanadium oxide single-crystalline nanobelts as a cathode material for lithium-ion batteries, Journal of Physical Chemistry B 110 (2006) 9383–9386.
[55] C. Yan, D. Xue, Formation of $Nb_2O_5$ nanotube arrays through phase transformation, Advanced Materials 20 (2008) 1055–1058.
[56] S. De, A. Dey, S.K. De, Characterization and transport properties of intercalated polypyrrole-vanadium pentoxide xerogel nanocomposite, Solid State Communications 137 (2006) 662–667.
[57] S. De, A. Dey, S.K. De, Electrical transport and optical properties of vanadyl phosphate-polyaniline nanocomposites, Journal of Physics and Chemistry of Solids 68 (2007) 66–72.
[58] G. Silversmit, D. Depla, H. Poelman, G.B. Marin, Determination of the V2p XPS binding energies for different vanadium oxidation states ($V^{5+}$–$V^{0+}$), Journal of Electron Spectroscopy and Related Phenomena 135 (2004) 167–175.
[59] J. Mendialdua, R. Casanova, Y. Barbaux, XPS studies of $V_2O_5$, $V_6O_{13}$, $VO_2$ and $V2O_3$, Journal of Electron Spectroscopy and Related Phenomena 71 (1995) 249–261.
[60] L. Soltane, F. Sediri, Hydrothermal synthesis, characterization and electrical investigation of poly(para-phenylenediamine)/vanadium oxide nanocomposite nanosheets, Materials Science and Engineering: B 178 (2013) 502–510.
[61] K.S.W. Sing, D.H. Everett, R.A.W. Haul, L. Moscou, R.A. Pierotti, J. Rouquerol, T. Siemieniewska, Reporting physisorption data for gas/solid systems with special reference to the determination of surface area and porosity, Pure and applied chemistry Chimie pure et appliquée 57 (1985) 603–619.